



Research article

UDC 69.04


DOI: 10.34910/MCE.121.5



Triangular prism finite element based on piecewise constant stress approximations

Yu. Ya. Tyukalov 

Vyatka State University, Kirov, Russian Federation

 yutvgu@mail.ru**Keywords:** finite element method, stress approximation, triangular prism, piecewise constant stresses, possible displacements, plates, beams

Abstract. The study object is a three-dimensional triangular prism finite element based on piecewise constant approximations of stresses. The use of such a finite element makes it possible to obtain more accurate stress values, especially at the boundaries of the region and in the stress concentration zones. The solution of the volume theory elasticity problem was obtained on the basis of the additional energy functional and the possible displacements principle. With the help of the possible displacement principle, algebraic equilibrium equations of finite element grid nodes are formed. The resulting equilibrium equations sum up with the additional energy of the system using the Lagrange multiplier method. In this case, the stresses are determined directly at the nodal points, and not at the finite element centers. The stress fields are continuous along finite element boundaries and discontinuous inside them. The paper shows that the displacements obtained by the proposed method, when refining the finite elements mesh, tend to exact values from above. As a test, the article provides calculations for bending plates and beams. As the test problems solutions showed, the proposed finite elements allow obtaining more accurate stress values compared to traditional finite elements based on stress approximation. Comparison of the stresses obtained by the proposed method with analytical solutions shows the high accuracy of the proposed method.

Citation: Tyukalov, Yu.Ya. Triangular prism finite element based on piecewise constant stress approximations. Magazine of Civil Engineering. 2023. 121(5). Article no. 12105. DOI: 10.34910/MCE.121.5

1. Introduction

The finite element method is the most popular method for solving various structural mechanics problems. Most of the developed finite elements are based on the displacements fields approximations. In this case, the stresses are determined through the derivatives of the displacement functions, are discontinuous along the finite element boundaries, and are determined for the finite element centers. Stresses are the most important characteristics, so it is necessary to determine them with greater accuracy. Therefore, development of the finite elements based on the stresses approximations is of relevance, as it will improve their calculation accuracy.

To date, numerous variants of finite elements have been developed for the calculation of rod systems, the elasticity theory plane problems, bending plates [1–3], shells and volume problems [4–7]. The papers [8–10] propose finite elements based on the stresses approximations. The solution is built on the basis of the additional energy functional, which is expanded by including the algebraic equilibrium equations of nodes in it using the Lagrange multipliers method [11, 12]. This approach makes it possible to more accurately determine the stress values, including stresses at nodal points. When solving such problems as the calculation of nodal connections of different sizes elements, the calculation of elements from dissimilar materials, the calculation of structures with a stepwise change in cross sections, a more accurate determination of stresses becomes essential. In this case, as a rule, maximum stresses occur at the subject area boundaries. To model such structures, it is necessary to use volumetric finite elements. In works [13–

17] for the stress-strain state analysis of reinforced concrete beams, columns and their connections, volumetric finite elements are used. In article [18] for the calculation of complex volumetric steel assemblies, variational formulations based on displacements and stresses are considered and the corresponding finite element discretization strategies are selected, giving, respectively, the upper and lower exact solution estimates. The proposed scheme is illustrated on the design of the torque transmission unit. To solve problems of plane elasticity theory, bending of plates and shells, a hybrid finite element formulations based on approximations of both displacements and stresses were used in articles [19–21]. Paper [21] notes that special hybrid elements are used to model the elements connection that do not lie in the same plane. These elements include the so-called plate elements and three-dimensional solid elements designed for the analysis of thin plates and shells. In articles [22, 23] for thermo-mechanical analysis of multilayer plates and shells the authors also used volumetric finite elements. It is noted that the proposed finite volumetric finite elements allow using only a few nodes in the thickness direction to obtain results with satisfactory accuracy. Article [24] investigates the behavior of steel-wood composite joints with bolted connectors embedded in grout pockets using 3D continuum finite element models. Finite element models are used to conduct a parametric study that investigates the effect of compressive strength of cement slurry, yield strength and shear size of bolted connectors, slurry size, pockets and the thickness of the steel profile flange on slippage characteristics under load, operational rigidity, peak load-bearing capacity and joint failure modes. To simulate the stress-strain state of bolted joints, various volumetric finite elements are widely used [25–28]. The volumetric finite elements are successfully used for modeling concrete and fiber-reinforced concrete structures [29–31]. Article [30] is aimed at evaluating the modulus of elasticity and Poisson's ratio of fiber-reinforced concrete using finite element modeling. A theoretical model for predicting the elastic modulus and Poisson's ratio of fiber-reinforced concrete was created using homogenization theory. To study the effect of local corrosion on the bearing capacity of long columns of round reinforced concrete steel pipes under eccentric compression, a numerical model was created using volumetric finite elements [32]. An eight-node 3d solid element of linear reduced integration is adopted for both the outer steel tube and the core concrete. The mesh element size is one tenth of the section diameter. The various volumetric finite elements are also being developed for the composite structures analysis by the finite element method [33, 34]. Various mixed formulations of the finite element method based on the additional energy and Reissner's functionals are developed in articles [35–38] to solve structural mechanics problems.

The review of scientific articles shows that the development and application of volumetric finite elements for the calculation of nodal connections and complex composite structures is relevant. Most of the finite elements currently used for this purpose are based on displacement approximations. This work aims to develop a volumetric triangular prism finite element based on stress approximation. The stresses obtained by the proposed method will be compared with analytical solutions and stresses calculated by the finite element method based on displacement approximation.

2. Methods

The solution to the bulk theory elasticity problem will be built based on the additional energy functional:

$$\Pi = \frac{1}{2} \int_V \left(\frac{1}{E} (\sigma_x^2 + \sigma_y^2 + \sigma_z^2) - \frac{\nu}{E} (\sigma_x \sigma_y + \sigma_x \sigma_z + \sigma_y \sigma_z) + \frac{1}{G} (\tau_{xy}^2 + \tau_{xz}^2 + \tau_{yz}^2) \right) dV. \quad (1)$$

E is the material elastic modulus; ν is Poisson's ratio, $G = 2(1 + \mu)/E$. We write the functional (1) in matrix form:

$$\Pi = \frac{1}{2} \int_V \boldsymbol{\sigma}^T \mathbf{E}^{-1} \boldsymbol{\sigma} dV, \quad (2)$$

$$\boldsymbol{\sigma}^T = (\sigma_x \quad \sigma_y \quad \sigma_z \quad \tau_{xy} \quad \tau_{xz} \quad \tau_{yz}),$$

$$\mathbf{E}^{-1} = \begin{bmatrix} 1/E & -\nu/E & -\nu/E & 0 & 0 & 0 \\ -\nu/E & 1/E & -\nu/E & 0 & 0 & 0 \\ -\nu/E & -\nu/E & 1/E & 0 & 0 & 0 \\ 0 & 0 & 0 & 1/G & 0 & 0 \\ 0 & 0 & 0 & 0 & 1/G & 0 \\ 0 & 0 & 0 & 0 & 0 & 1/G \end{bmatrix}.$$

Fig. 1 shows a triangular prism finite element and six marked regions with constant stresses. In each region, the stresses are constant and equal to the stresses in the corresponding finite element node.

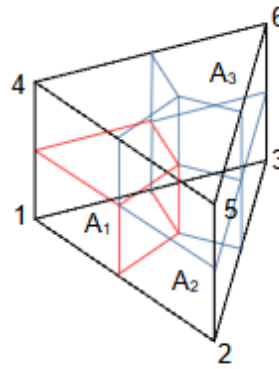


Figure 1. Triangular prism finite element.

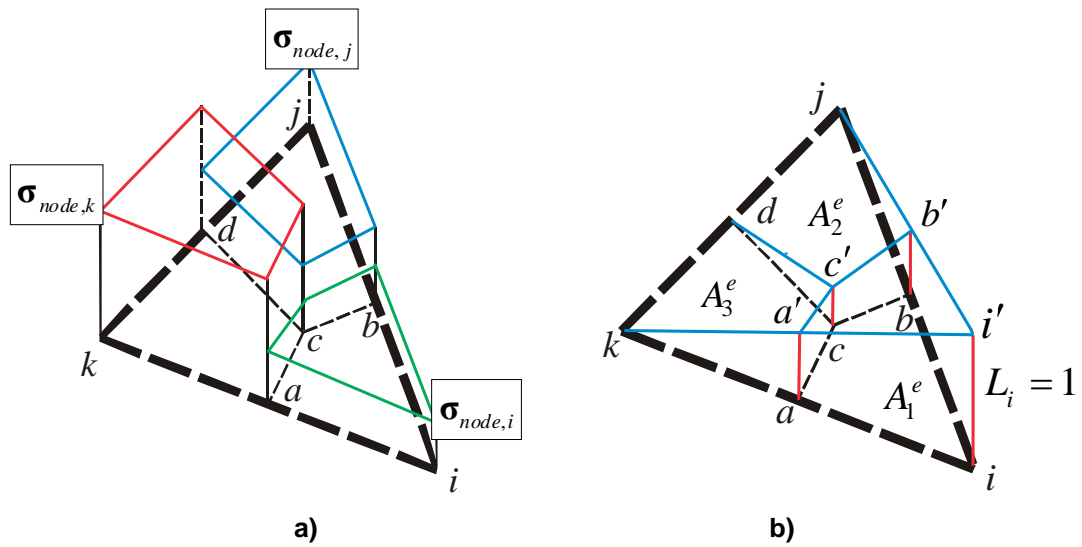


Figure 2. a) stresses distribution; b) triangular coordinate.

The red lines restrict the prism region with stresses, which equal the stresses on node 1. A_1, A_2, A_3 are the squares of prism bottoms and covers. Let us denote the nodal unknown stresses vector, in a global coordinate system, as

$$\sigma_{node,k}^T = (\sigma_{x,k} \quad \sigma_{y,k} \quad \sigma_{z,k} \quad \tau_{xy,k} \quad \tau_{xz,k} \quad \tau_{yz,k}). \quad (3)$$

Vector of finite element unknown stresses is

$$\sigma_{el,k}^T = (\sigma_{node,1}^T \quad \sigma_{node,2}^T \quad \dots \quad \sigma_{node,6}^T). \quad (4)$$

To simplify the notation, let us introduce unit step functions and diagonal matrices

$$h_i(x, y, z) = \begin{cases} 1, & (x, y, z) \in V_i \\ 0, & (x, y, z) \notin V_i \end{cases}, \quad \mathbf{H}_i = \begin{bmatrix} h_i & & \\ & h_i & \\ & & h_i \end{bmatrix}. \quad (5)$$

Then the approximation matrix of stresses in the finite element volume will have the simple form (Fig. 1b):

$$\mathbf{Z}_k = [\mathbf{H}_1 \quad \mathbf{H}_2 \quad \dots \quad \mathbf{H}_6], \quad \sigma = \mathbf{Z}_k \sigma_{el,k}. \quad (6)$$

Using (4)–(6), we express the finite element additional energy in the following form:

$$\Pi_k = \int_{V_k} \sigma_{el,k}^T (\mathbf{Z}_k^T \mathbf{E}_k^{-1} \mathbf{Z}_k) \sigma_{el,k} dV. \quad (7)$$

The pliability matrix of the finite element is

$$\mathbf{D}_k = \int_{V_k} \mathbf{Z}_k^T \mathbf{E}_k^{-1} \mathbf{Z}_k dV. \tag{8}$$

The matrix has a simple block-diagonal form. Global matrix \mathbf{D} of the whole system is formed from local finite elements matrices. Functional (1) of the whole system:

$$\Pi = \frac{1}{2} \boldsymbol{\sigma}_V^T \mathbf{D} \boldsymbol{\sigma}_V. \tag{9}$$

$\boldsymbol{\sigma}_V$ is a global vector of the unknown stresses of the system.

Global matrix \mathbf{D} has a block-diagonal form:

$$\mathbf{D} = \begin{bmatrix} \mathbf{d}_1 & & & & & \\ & \mathbf{d}_2 & & & & \\ & & \ddots & & & \\ & & & \mathbf{d}_i & & \\ & & & & \ddots & \\ & & & & & \mathbf{d}_n \end{bmatrix}. \quad \mathbf{d}_i = \frac{1}{6} \sum_k V_{i,k} \mathbf{E}_k^{-1}. \tag{10}$$

n is number of system nodes; $V_{i,k}$ and k are the volume and index of finite elements adjoining node i .

\mathbf{E}_k^{-1} is material stiffness matrix of finite element k .

Denote the nodal unknown stresses vector, in local coordinate system (Fig. 3), as

$$\bar{\boldsymbol{\sigma}}_{node,k}^T = (\bar{\sigma}_{x,k} \quad \bar{\sigma}_{y,k} \quad \bar{\sigma}_{z,k} \quad \bar{\tau}_{xy,k} \quad \bar{\tau}_{xz,k} \quad \bar{\tau}_{yz,k}). \tag{11}$$

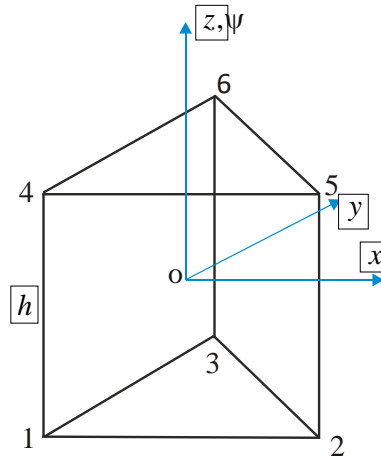


Figure 3. Local coordinate system.

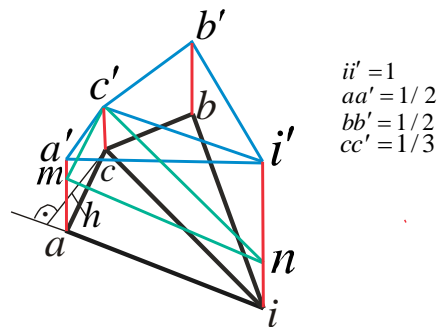


Figure 4. Integration of a triangular coordinate.

In accordance with the minimum additional energy principle, the stress functions must satisfy the equilibrium equations. Therefore, using the possible displacements principle, we will obtain algebraic equations for the nodes equilibrium along the coordinate axes. As a result, we will have the problem of minimizing the additional energy functional in the presence of constraints in the equations system form. We will solve such problem by the Lagrange multipliers method. It should be noted, that such functional is not a mixed one, in which both stress and displacement approximations are used simultaneously. The proposed solution only uses the approximations of possible displacement when we obtain the equilibrium equations. As known, approximations of possible displacements can be any functions that satisfy the boundary kinematic conditions.

To obtain the equilibrium equations, we give possible node displacements along the local coordinate axes (Fig. 3):

$$\begin{aligned}\delta\bar{u}_i &= u_0 \frac{1}{2} L_i (1 + \psi \psi_i), \quad \delta\bar{v}_i = v_0 \frac{1}{2} L_i (1 + \psi \psi_i), \\ \delta\bar{w}_i &= w_0 \frac{1}{2} L_i (1 + \psi \psi_i), \quad i = 1, 2, \dots, 6.\end{aligned}\quad (12)$$

$$\psi = \frac{2z}{h^e}, \quad L_i = \frac{1}{2A} (a_i + b_i x + c_i y), \quad (13)$$

$$a_i = x_{i+1}y_{i+2} - x_{i+2}y_{i+1}, \quad b_i = y_{i+1} - y_{i+2}, \quad c_i = x_{i+2} - x_{i+1}.$$

Parameters u_0 , v_0 , w_0 are introduced for the convenience of the transition to the global coordinate system and below are taken equal to 1. Possible displacements of node i along the x axis give the following deformations of the finite elements adjacent to this node:

$$\begin{aligned}\delta\varepsilon_x &= \frac{\partial(\delta\bar{u}_i)}{\partial x} = \frac{b_i}{4A^e} (1 + \psi \psi_i), \quad \delta\gamma_{xy} = \frac{\partial(\delta\bar{u}_i)}{\partial y} = \frac{c_i}{4A^e} (1 + \psi \psi_i), \\ \delta\gamma_{xz} &= \frac{\partial(\delta\bar{u}_i)}{\partial z} = \frac{\psi_i L_i}{h^e}.\end{aligned}\quad (14)$$

A^e is bottom area of a triangular prism. The possible finite element strain energy

$$\delta\bar{U}_{i,x}^e = \int_0^{h^e} \int_{A^e} (\bar{\sigma}_x \delta\varepsilon_x + \bar{\tau}_{xy} \delta\gamma_{xy} + \bar{\tau}_{xz} \delta\gamma_{xz}) dAdz. \quad (15)$$

Using (14), let us get

$$\delta\bar{U}_{i,x}^e = \frac{h^e}{2} \sum_{J=1-1}^6 \int_{A_J^e} \left(\frac{b_i (1 + \psi \psi_i)}{4A^e} \bar{\sigma}_{x,j} + \frac{c_i (1 + \psi \psi_i)}{4A^e} \bar{\tau}_{xy,j} + \frac{\psi_i L_i}{d^e} \bar{\tau}_{xz,j} \right) dAd\psi. \quad (16)$$

The first two terms integration in (16) does not cause difficulties. To calculate the third term, it is necessary to integrate the linear function over triangular areas. Fig. 2b shows graphs of stress changes and a linear function over the prism base area. In Fig. 2, points a , b , d bisect the corresponding sides.

Point c has triangular coordinates $L_i = L_j = L_k = 1/3$. Function L_i integral over the area A_1^e is equal to the volume of the figure $acbia'c'b'i'$. This figure can be divided into two equal parts by the plane $cc'ii'$ (Fig. 4). The triangles areas aci and cbi are equal. In Fig. 4, lines $c'n$ and $c'm$ are parallel to the base. The $aciac'i'$ volume can be represented as the sum of a triangular prism $acimc'n$ volume and a pyramid $c'ma'ni'$ volume. Then

$$\int_{A_1^e} L_i dA = 2 \left(\frac{1}{3} \cdot \frac{A^e}{6} + \frac{1}{3} h \cdot mn \cdot \frac{\left(\frac{1}{6} + \frac{2}{3}\right)}{2} \right) = \frac{11}{54} A^e. \quad (17)$$

Product $h \cdot mn = \frac{A^e}{3}$. Function L_i integral over the area A_2^e is equal to the sum of the pyramid's volumes $jdcc'$ and $jcc'bb'$. Let us get

$$\int_{A_2^e} L_i dA = \frac{1}{3} \cdot h_1 \cdot dc \cdot \frac{1}{2} \cdot cc' + \frac{1}{3} \cdot h_2 \cdot cb \cdot \frac{1}{2} (cc' + bb') = \frac{7}{108} A^e. \quad (18)$$

In (18), h_1 , h_2 are the heights lowered from point j to cd and cb , respectively. Considering (17) and (18), we get

$$\delta \bar{U}_{i,x}^e = \sum_{j=1}^6 \left(\frac{h^e b_i (1 + \psi_i \psi_j / 2)}{24} \bar{\sigma}_{x,j} + \frac{h^e c_i (1 + \psi_i \psi_j / 2)}{24} \bar{\tau}_{xy,j} + \frac{k_{ij} \psi_i A^e}{216} \bar{\tau}_{xz,j} \right). \quad (19)$$

If $(i = j) \vee (i = j + 3) \vee (i = j - 3)$ $k_{ij} = 22$, else $k_{ij} = 7$. The strain energy of finite element with a node possible displacement along the Y and Z axes is written by analogy:

$$\delta \bar{U}_{i,y}^e = \sum_{j=1}^6 \left(\frac{h^e c_i (1 + \psi_i \psi_j / 2)}{24} \bar{\sigma}_{y,j} + \frac{h^e b_i (1 + \psi_i \psi_j / 2)}{24} \bar{\tau}_{xy,j} + \frac{k_{ij} \psi_i A^e}{216} \bar{\tau}_{yz,j} \right), \quad (20)$$

$$\delta \bar{U}_{i,z}^e = \sum_{j=1}^6 \left(\frac{h^e b_i (1 + \psi_i \psi_j / 2)}{24} \bar{\tau}_{xz,j} + \frac{h^e c_i (1 + \psi_i \psi_j / 2)}{24} \bar{\tau}_{yz,j} + \frac{k_{ij} \psi_i A^e}{216} \bar{\sigma}_{z,j} \right). \quad (21)$$

Expression (19)–(21) let us write in matrix form:

$$\delta \mathbf{U}_i^e = \begin{cases} \delta \bar{U}_{i,x}^e \\ \delta \bar{U}_{i,y}^e \\ \delta \bar{U}_{i,z}^e \end{cases} = \delta \bar{\mathbf{u}}_i^e \bar{\mathbf{L}}_i^e \bar{\boldsymbol{\sigma}}^e, \quad \delta \bar{\mathbf{u}}_i^e = \begin{bmatrix} u_0 & 0 & 0 \\ 0 & v_0 & 0 \\ 0 & 0 & w_0 \end{bmatrix}. \quad (22)$$

Let us express the stresses and possible displacements $\bar{\boldsymbol{\sigma}}^e$, $\delta \bar{\mathbf{u}}_i^e$ in the local coordinate system in terms of the corresponding parameters $\boldsymbol{\sigma}^e$, $\delta \mathbf{u}_i^e = 1$ in the global system:

$$\bar{\boldsymbol{\sigma}}^e = \mathbf{C}_\sigma \boldsymbol{\sigma}^e, \quad \delta \bar{\mathbf{u}}_i^e = \mathbf{C}_u \delta \mathbf{u}_i^e. \quad (23)$$

The transition matrices \mathbf{C}_σ , \mathbf{C}_u have a standard form. Substituting (23) into (22), we get

$$\delta \mathbf{U}_i^e = \delta \mathbf{u}_i^e \mathbf{L}_i^e \boldsymbol{\sigma}^e, \quad \mathbf{L}_i^e = \mathbf{C}_u^T \bar{\mathbf{L}}_i^e \mathbf{C}_\sigma. \quad (24)$$

The external forces potential with the node possible displacements in the global coordinate system will have the following form:

$$\delta \mathbf{V}_i^e = \delta \mathbf{u}_i^e \mathbf{P}_i^e. \quad (25)$$

From matrices \mathbf{L}_i^e of all finite elements nodes "equilibrium" matrix \mathbf{L} for all system is formed. Matrix \mathbf{L} rows number is equal to the number of system nodes possible displacements, and the columns number

is equal to the the total number of nodal unknown stresses. The matrix has a band structure of non-zero elements. Global load vector \mathbf{P} is formed from vectors \mathbf{P}_i^e of all finite elements nodes.

Let us take the algebraic equations system for the equilibrium of nodes in matrix form:

$$\mathbf{L}\sigma_V + \mathbf{P} = 0. \quad (26)$$

σ_V is the vector of the node's stresses for the whole system. Using the Lagrange multipliers method, we add the equilibrium equations to functional (9):

$$\Pi = \frac{1}{2} \sigma_V^T \mathbf{D} \sigma_V + \mathbf{w}^T (\mathbf{L} \sigma_V + \mathbf{P}) \rightarrow \min. \quad (27)$$

\mathbf{w} is the nodes displacements vector.

Equating the functional derivatives with respect to σ_V and \mathbf{w} to zero, we obtain the system of equations:

$$\mathbf{D} \sigma_V + \mathbf{w}^T \mathbf{L} = 0, \quad \mathbf{L} \sigma_V + \mathbf{P} = 0. \quad (28)$$

We express vector σ_V from the first matrix equation and put it into the second one. Then we get

$$\sigma_V = -\mathbf{L}^T \mathbf{D}^{-1} \mathbf{w}, \quad \mathbf{K} = -\mathbf{L}^T \mathbf{D}^{-1} \mathbf{L}, \quad \mathbf{K} \mathbf{w} = \mathbf{P}. \quad (29)$$

\mathbf{K} is the whole system stiffness matrix. That matrix also has a band structure of the non-zero elements. Matrix \mathbf{D} has a block-diagonal structure and is inversed analytically. When calculating product $\mathbf{L}^T \mathbf{D}^{-1} \mathbf{L}$, the band structure of non-zero elements of matrix \mathbf{L} is taken into account. Solving the equations system, we determine the nodal displacements, and then calculate the nodal stresses (24). Thus, the stress fields are continuous along element boundaries and discontinuous inside ones. On the contrary, when using the finite element method based on the displacement approximations, the stress fields are continuous inside the finite elements and discontinuous along their boundaries.

3. Results and Discussions

To test the method, a pinched beam (Fig. 5) and a hinged plate (Fig. 6) calculations were performed. Such tasks were chosen because there are analytical solutions for them.

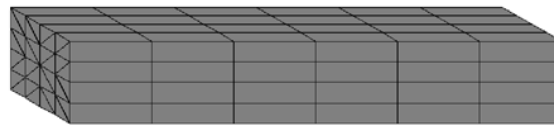


Figure 5. Finite element model of a pinched beam.

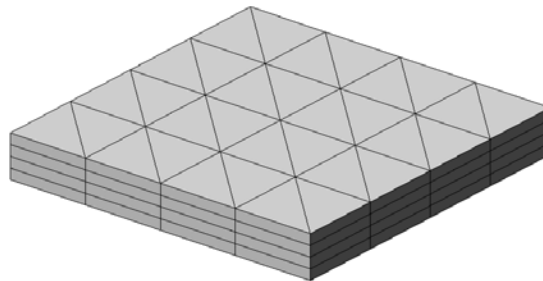


Figure 6. Finite element model of a hinged plate (quarter).

The beam length is 6 meters, the cross-section dimensions are 1 by 1 meter. The material elasticity modulus is 10^6 kN/m². A uniformly distributed vertical load $q = 1$ kN/m² is applied to the cross section at the beam free end. Options for the beam cross section dividing into the finite elements are shown in Fig. 7. The beam length was divided into six (for schemes in Fig. 7a and Fig. 7b) or twelve (for scheme in Fig. 7c) finite elements. The square hinged plate measures 6 by 6 meters and is 0.4 meters thick. The load on the plate is evenly distributed $q = 1$ kN/m². Poisson's ratio is $\mu = 0.3$.

According to the thickness, the plate is divided into 4 finite elements for variants in Fig. 9a, Fig. 9b and into 6 elements for the variant in Fig. 9c. The calculation results in the figures and the table, obtained by the proposed method, are indicated as FEM-S, and the results obtained by LIRA-SAPR program, which use the traditional finite elements, are indicated as FEM-D.

An analytical solution for the hinged plate was obtained in [39]. According to it, the displacement and the bending moment in the plate center are determined by the following expressions:

$$M = 0.0479qa^2, \quad w = \frac{0.00496qa^4}{Eh^3/12(1-\mu^2)}. \quad (30)$$

The analytical values of the plate center displacement and the outer fiber stress are given in Table 1. An analytical solution for the cantilever beam is easily obtained based on Kirchhoff's beam bending theory.

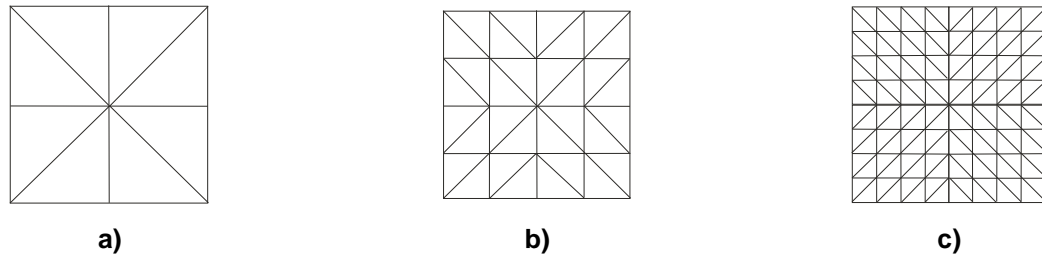


Figure 7. Dividing the beam cross section into finite elements.

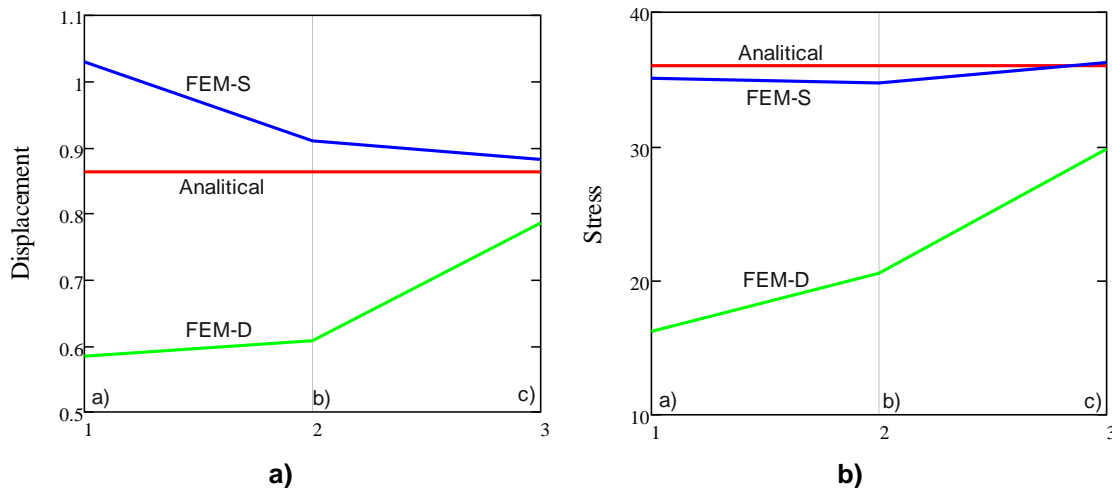


Figure 8. Displacements and stresses of the pinched beam.

Table 1. Displacements and stresses.

Grid	Displacements, mm				Stresses, kN/m ²			
	Free end of the beam		Center of the plate		Pinched end of the beam		Center of the plate	
	FEM-S	FEM-D	FEM-S	FEM-D	FEM-S	FEM-D	FEM-S	FEM-D
a)	1.029	0.585	0.835	0.173	35.08	16.20	42.38	8.275
b)	0.911	0.608	1.030	0.439	34.70	20.50	49.76	25.00
c)	0.883	0.785	1.010	0.729	36.22	29.81	59.24	48.00
Analytical	0.864		0.898		36.0		64.625	

An analysis of the calculation results of the pinched beam shows that when grinding the finite element meshes, with stress piecewise constant approximations, the stresses converge with the exact values from above. In addition, the displacements obtained by the finite element method, based on the displacement approximations, approach the exact values from below. Thus, in terms of displacements, we have two alternative solutions. Similar results were obtained using the finite elements based on piecewise constant stress approximations for the bending plates and the flat theory of elasticity [8, 9].

Moreover, the displacements and stresses values obtained by the proposed method are more accurate than the values calculated by the traditional finite element method based on displacement approximation. For example, the stresses obtained with the finest mesh by the displacement approximation

method are 17% less than the analytical value, and the stresses obtained by the proposed method practically coincide with the exact value. The deviation of the displacement value obtained by the FEM–S method from the analytically obtained one is 2%, and the displacement obtained by the FEM–D method deviates from the exact value by 9%.

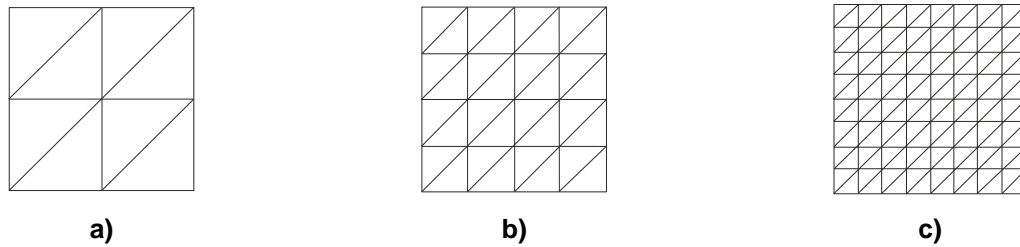


Figure 9. Division of the plate quarter into finite elements.

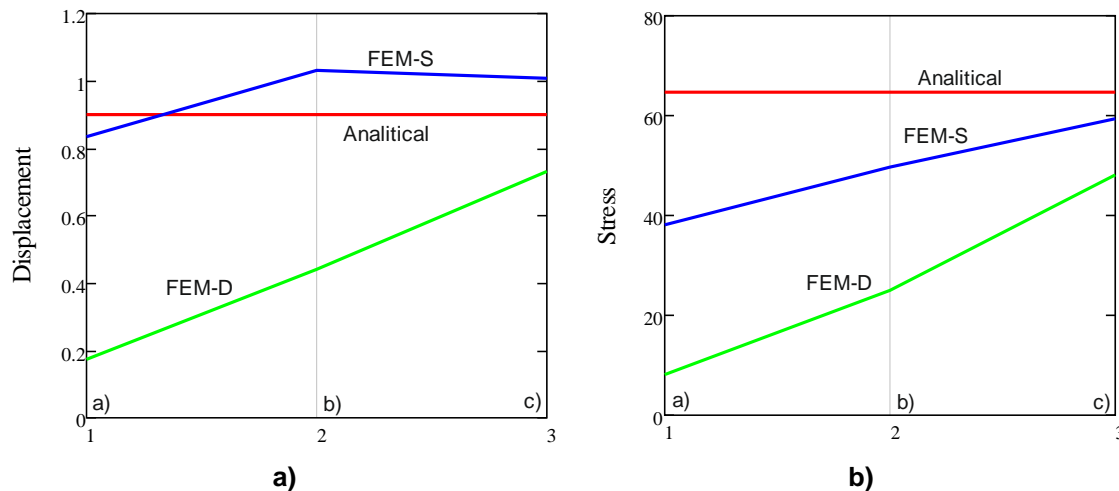


Figure 10. Displacements and stresses of the hinged plate center.

When analyzing the square hinged plate calculating results for a uniformly distributed load, the same trends are observed (Fig. 10). For the finite element mesh shown in Fig. 9c, the displacements obtained by the FEM-S method are 12% more than the analytical value, and the displacements obtained by the FEM-D method are 19% less. In addition, the displacement values obtained by the FEM-S method, when the finite element mesh is refined, approach the exact value from above. The stresses at the plate center, obtained by the FEM-S method, are also more accurate and differ from the analytical value by 8 percent. The stresses obtained by the FEM-D method are less than the analytical value by 26%.

At present, volumetric finite elements are increasingly used to calculate such problems as nodal connections, connections of columns and slabs, and calculation of variable section elements. In such structures, points and areas of increased stresses arise, which, as a rule, are located at the edges and boundaries of the areas. In such cases, the use of the proposed finite elements, based on piecewise constant approximations, will allow more accurate determination of the structure stress-strain state, and, accordingly, increase the design solutions reliability.

4. Conclusion

1. The volumetric triangular prism finite element based on piecewise constant approximations of stresses is presented. The stress fields are continuous along finite element boundaries and discontinuous inside them. The solution of the volume theory elasticity problem was obtained on the basis of the additional energy functional and the possible displacements principle.

2. The displacements obtained by the proposed method, when refining the finite elements mesh, tend to exact values from above; they are more accurate than the values obtained by the finite element method in displacements.

3. As the test problems solutions showed, the proposed finite elements allow obtaining more accurate stress values compared to traditional finite elements based on displacements approximations. In this method, the stresses are determined directly at the nodal points, and not at the finite element centers. For the first example, the stresses obtained with the finest mesh by the displacement approximation method are 17 percent less than the analytical value, and the stresses obtained by the proposed method practically coincide with the exact value. For the second task, the stresses at the plate center, obtained by the

proposed method, are also more accurate and differ from the analytical value by 8% and the stresses obtained by the finite element method in displacement are 26% less than the analytical value.

References

1. Cho, J.R. Natural element approximation of hierarchical models of plate-like elastic structures. *Finite Elements in Analysis and Design*. 2020. 180(September). Pp. 103439. DOI: 10.1016/j.finel.2020.103439
2. Du, L., Qi, J., Cheng, Z., Wang, J. Finite element modeling of UHPC slabs with dovetail joints and steel wire mesh using an innovative interfacial treating method. *Structures*. 2022. 37 (January). Pp. 745–755. DOI: 10.1016/j.istruc.2022.01.057
3. Abdikarimov, R., Amabili, M., Vatin, N.I., Khodzhaev, D. Dynamic stability of orthotropic viscoelastic rectangular plate of an arbitrarily varying thickness. *Applied Sciences (Switzerland)*. 2021. 11 (13). DOI: 10.3390/app11136029
4. Gao, X.-W., Gao, L.-F., Zhang, Y., Cui, M., Lv, J. Free element collocation method: A new method combining advantages of finite element and mesh free methods. *Computers & Structures*. 2019. 215. Pp. 10–26. DOI: 10.1016/j.compstruc.2019.02.002
5. Genikomsou, A.S., Polak, M.A. 3D finite element investigation of the compressive membrane action effect in reinforced concrete flat slabs. *Engineering Structures*. 2017. 136. Pp. 233–244. DOI: 10.1016/j.engstruct.2017.01.024
6. Judge, R., Yang, Z., Jones, S.W., Beattie, G. Full 3D finite element modelling of spiral strand cables. *Construction and Building Materials*. 2012. 35. Pp. 452–459. DOI: 10.1016/j.conbuildmat.2011.12.073.
7. Kebir, H., Zouari, W., Assarar, M., Ayad, R. A specific eight-node hexahedral finite element for the analysis of 3D fibre-reinforced composites. *Composite Structures*. 2023. 303. Pp. 110456. DOI: 10.1016/j.compstruct.2022.116269.
8. Tyukalov, Y.Y. Calculation of bending plates by finite element method in stresses. *IOP Conference Series: Materials Science and Engineering*. 2018. 451 (1). DOI: 10.1088/1757-899X/451/1/012046
9. Tyukalov, Y.Y. Calculation of circular plates with assuming shear deformations. *IOP Conference Series: Materials Science and Engineering*. 2019. 687 (3). DOI: 10.1088/1757-899X/687/3/033004
10. Tyukalov, Y.Y. Method of plates stability analysis based on the moments approximations. *Magazine of Civil Engineering*. 2020. 95 (3). Pp. 90–103. DOI: 10.18720/MCE.95.9
11. Tyukalov, Y.Y. Arbitrary quadrangular finite element for plates with shear deformations. *Magazine of Civil Engineering*. 2021. 107 (7). DOI: 10.34910/MCE.107.7
12. Tyukalov, Y.Y. Equilibrium finite elements for plane problems of the elasticity theory. *Magazine of Civil Engineering*. 2019. 91 (7). Pp. 80–97. DOI: 10.18720/MCE.91.8.
13. Chen, Z., Chen, J., Jiang, X., Mo, L. Experimental research and finite element analysis on seismic behavior of square reinforced concrete columns with four interlocking spirals. *Structures*. 2022. 39 (March). Pp. 1–16. DOI: 10.1016/j.istruc.2022.03.023
14. Izadi, A., Teh, L.H., Polak, M.A., Ahmed, A. Finite element analysis of square FRP-Concrete-Steel columns under concentric compression. *Structures*. 2022. 44 (August). Pp. 1312–1320. DOI: 10.1016/j.istruc.2022.08.051
15. Li, D. bin, Chai, Y. kai, Li, W. long, Xiang, R. Experimental study and finite element analysis of seismic behaviour of novel precast prestressed concrete frames. *Structures*. 2022. 38 (December 2020). Pp. 402–415. DOI: 10.1016/j.istruc.2022.02.019
16. Raza, A., Rehman, A. ur, Masood, B., Hussain, I. Finite element modelling and theoretical predictions of FRP-reinforced concrete columns confined with various FRP-tubes. *Structures*. 2020. 26 (March). Pp. 626–638. DOI: 10.1016/j.istruc.2020.04.033
17. Shoaib Karam, M., Nakamura, H., Yamamoto, Y., Miura, T. Numerical evaluation of the perfbond (PBL) shear connector with transverse rebar using coupled rigid Body spring model (RBSM) and solid finite element method (FEM). *Structures*. 2022. 45 (October). Pp. 1544–1560. DOI: 10.1016/j.istruc.2022.09.117
18. Boustani, C. El, Bleyer, J., Arquier, M., Ferradi, M.K., Sab, K. Elastoplastic and limit analysis of 3D steel assemblies using second-order cone programming and dual finite-elements. *Engineering Structures*. 2020. 221 (May). Pp. 111041. DOI: 10.1016/j.engstruct.2020.111041
19. Zhou, J., Wang, K., Li, P. A hybrid fundamental-solution-based 8-node element for axisymmetric elasticity problems. *Engineering Analysis with Boundary Elements*. 2019. 101. Pp. 297–309. DOI: 10.1016/j.enganabound.2019.01.015
20. Góis, W., Proença, S.P.B. Generalized Finite Element Method on Hybrid Stress Approach: Formulation and Numerical Performance. *Buenos Aires*. 2010. XXIX. Pp. 4687–4705.
21. Pian, T.H.H., Sze, K.-Y. Hybrid Stress Finite Element Methods for Plate and Shell Structures. *Advances in Structural Engineering*. 2003. 4 (1). Pp. 13–18. DOI: 10.1260/1369433011502309
22. Liu, B., Lu, S., Ji, J., Ferreira, A.J.M., Liu, C., Xing, Y. Three-dimensional thermo-mechanical solutions of cross-ply laminated plates and shells by a differential quadrature hierarchical finite element method. *Composite Structures*. 2019. 208 (May 2018). Pp. 711–724. DOI: 10.1016/j.compstruct.2018.10.022
23. Liu, B., Lu, S., Wu, Y., Xing, Y. Three dimensional micro/macro-mechanical analysis of the interfaces of composites by a differential quadrature hierarchical finite element method. *Composite Structures*. 2017. 176. Pp. 654–663. DOI: 10.1016/j.compstruct.2017.05.068
24. Hassanieh, A., Valipour, H.R., Bradford, M.A. Bolt shear connectors in grout pockets: Finite element modelling and parametric study. *Construction and Building Materials*. 2018. 176. Pp. 179–192. DOI: 10.1016/j.conbuildmat.2018.05.029
25. Liu, T., Lu, J., Wang, D., Liu, H., Mo, N., Zhai, L. 3D nonlinear finite element modelling of mechanical behavior of a new wall-beam-strut joint for prefabricated underground construction and validation again experimental testing. *Structures*. 2021. 33 (December 2019). Pp. 3202–3221. DOI: 10.1016/j.istruc.2021.06.059
26. Liu, Z., Yan, X., Zheng, M., Wang, Y., Chen, W., Li, Y. The effect of tightening again on bolt loosening under transverse load: Experimental and finite element analysis. *Structures*. 2022. 44 (August). Pp. 1303–1311. DOI: 10.1016/j.istruc.2022.08.049
27. Najafgholipour, M.A., Sarhadi, F. A finite element study on the ultimate lateral drift capacity of interior reinforced concrete flat slab-column connections. *Structures*. 2022. 46 (November). Pp. 913–926. DOI: 10.1016/j.istruc.2022.10.128
28. Zhao, J., Wang, Z., Qian, F., Peng, Y., Dong, J. Finite element analysis of the shear capacity of stainless-steel screw connections. *Structures*. 2022. 41 (May). Pp. 957–968. DOI: 10.1016/j.istruc.2022.05.048

29. Li, Y., Guan, Z., Wang, Z., Wang, P., Li, Y., Zhang, G., Ding, Q. 3D meso-scale finite element modelling on cement paste corroded in sodium sulfate with X-ray CT technique. *Construction and Building Materials*. 2019. 202. Pp. 727–737. DOI: 10.1016/j.conbuildmat.2019.01.020
30. Li, Y., Li, Y. Evaluation of elastic properties of fiber reinforced concrete with homogenization theory and finite element simulation. *Construction and Building Materials*. 2019. 200. Pp. 301–309. DOI: 10.1016/j.conbuildmat.2018.12.134
31. Xu, R., Bouby, C., Zahrouni, H., Ben Zineb, T., Hu, H., Potier-Ferry, M. 3D modeling of shape memory alloy fiber reinforced composites by multiscale finite element method. *Composite Structures*. 2018. 200 (May). Pp. 408–419. DOI: 10.1016/j.compstruct.2018.05.108
32. Wang, K., Chen, M., Zhang, R., Fang, W. Finite element simulation of load bearing capacity of circular CFST long columns with localized corrosion under eccentric load. *Structures*. 2022. 43 (August). Pp. 1629–1642. DOI: 10.1016/j.istruc.2022.07.029
33. Ye, J., Yan, Y., Li, J., Hong, Y., Tian, Z. 3D explicit finite element analysis of tensile failure behavior in adhesive-bonded composite single-lap joints. *Composite Structures*. 2018. 201 (May). Pp. 261–275. DOI: 10.1016/j.compstruct.2018.05.134
34. Nguyen, M.N., Bui, T.Q., Truong, T.T., Tanaka, S., Hirose, S. Numerical analysis of 3-D solids and composite structures by an enhanced 8-node hexahedral element. *Finite Elements in Analysis and Design*. 2017. 131. Pp. 1–16. DOI: 10.1016/j.finel.2017.04.002
35. Lukashovich, A.A., Lukashovich, N.K. Numerical solution of contact problems with friction under dynamic loads. *IOP Conference Series: Materials Science and Engineering*. 2020. Vol. 753. 022058. DOI: 10.1088/1757-899X/753/2/022058
36. Lukashovich, A.A. Finite element models based on the approximation of discontinuous stress fields. *Magazine of Civil Engineering*. 2022. 110 (2). Article No. 11004. DOI: 10.34910/MCE.110.4
37. Lalin, V.V., Rybakov, V.A., Ivanov, S.S., Azarov, A.A. Mixed finite-element method in Slivker's semi-shear thin-walled bar theory. *Magazine of Civil Engineering*. 2019. 89 (5). Pp. 79–93. DOI: 10.18720/MCE.89.7
38. Ignatyev, A.V., Ignatyev, V.A. On the efficiency of the finite element method in the form of the classical mixed method. *Procedia Engineering*. 2016. Vol. 150. Pp. 1760–1765. DOI: 10.1016/j.proeng.2016.07.167
39. Timoshenko, S.P., Voinovskiy-Kriger, S. *Plastiny i obolochki [Plates and shells]*. Moscow : Nauka, 1966. 636 p.

Information about author:

Yury Tyukalov, Doctor of Technical Sciences

ORCID: <https://orcid.org/0000-0001-6184-2365>

E-mail: yutvgu@mail.ru

Received 31.01.2023. Approved after reviewing 22.05.2023. Accepted 29.05.2023.